NORTHWESTERN
UNIVERSITY

Center for Science and Protection of Engineered Environments (SPREE)

Department of Civil and Environmental Engineering

McCormick School of Engineering and Applied Science

Evanston, Illinois 60208, USA

On the collapse of the Medici masonry tower: an integrated discrete-analytical approach

Micaela Mercuri, Madura Pathirage, Amedeo Gregori, Gianluca Cusatis

SPREE INTERNAL REPORT No. 21-6/001S

Submitted to Engineering Structures *March 2021*

On the collapse of the Medici masonry tower: an integrated discrete-analytical approach

By

Micaela Mercuri [1], Madura Pathiragei [2], Amedeo Gregori [3], Gianluca Cusatis* [4]

A Paper Submitted to

Engineering Structures

March 2, 2021

Corresponding Author

Amedeo Gregori

Associate Professor

Department of Civil, Construction-Architecture and Environmental Engineering

University of L'Aquila

Via Giovanni Gronchi 18, Zona Industriale di Pile

67100 L'Aquila, Italy

E-mail: amedeo.gregori@univaq.it

[1]Department of Civil, Construction-Architecture and Environmental Engineering, L'Aquila, Italy.

[2]Department of Civil and Environmental Engineering, Northwestern University, Evanston, IL, USA.

[3]Corresponding author. Postal address: Department of Civil, Construction-Architecture and Environmental Engineering, University of L'Aquila, Via Giovanni Gronchi 18, Zona Industriale di Pile, 67100 L'Aquila, Italy. E-mail: amedeo.gregori@univaq.it

[4]Department of Civil and Environmental Engineering, Northwestern University, Evanston, IL, USA.

On the collapse of the Medici masonry tower: an integrated discrete-analytical approach.

Micaela Mercuri[a], Madura Pathirage[b], Amedeo Gregori[a], Gianluca Cusatis[b,*]

[a]*Department of Civil, Building and Environmental Engineering, University of L'Aquila, L'Aquila, Italy*
[b]*Department of Civil and Environmental Engineering, Northwestern University, Evanston, IL, USA*

Abstract

Masonry towers are characterized by a high susceptibility to seismic actions. Different approaches exist to study their mechanical behavior and are used depending on the desired level of accuracy of the analysis. Construction codes usually requires the study of local and global collapse mechanisms based on simplified kinematic analysis. The identification of the correct collapse configuration is however complex and necessitates thorough on-site surveys. More elaborated approaches such as finite element method are also performed to simulate the response of masonry towers. Although successful in many applications, these methods are limited in accurately capturing crack distributions and fracture mechanisms. In this work, an integrated discrete-analytical approach is proposed. First, the Lattice Discrete Particle Model (LDPM), which simulates masonry at the stone level and has a superior capability in capturing fracture processes, is adopted to simulate masonry towers subjected to seismic excitation. The numerical model is used to predict the actual collapse mechanism. Next, the final fractured configuration is used in the kinematic analysis for the calculation of the ultimate condition. The proposed method is used to analyze the collapse of the Medici tower that was subjected to the 2009 L'Aquila earthquake. The induced damage and the crack contours are simulated. Six different failure configurations are then assumed for the kinematic analysis taking into account the relative position of the openings and the fracture locations. Results show that the collapse of the Medici tower is well replicated by LDPM and the corresponding kinematic analyses demonstrate the efficiency of the proposed hybrid approach applied to this case study. The paper also shows that different load configurations, more specifically the direction of the seismic action, result in more diffused damage states and clear failure patterns cannot be identified for kinematic analyses. In these cases, it appears fundamental to rely mainly on comprehensive numerical models, such as LDPM, to study the fracturing process from the cracks trigger to the ultimate complex collapse mechanism.

Keywords: Earthquake, Tower, Unreinforced Irregular Masonry, Lattice Discrete Particle Model, Fracture Mechanics, Cohesive Behavior, Non-Linear Analysis, Kinematic Analysis, Local Collapse Mechanisms, Global Collapse Mechanisms

1. Introduction

Masonry towers represent one of the most relevant architectural category composing the world cultural heritage [2, 3, 4]. Particularly, numerous Italian medieval towns are connoted by the presence of civic towers soaring in the urban skyline [5, 6, 7]. On the other hand, unreinforced masonry tall buildings are characterized by high susceptibility to seismic actions [8, 9]. By way of illustration, Fig. 1 shows three examples of towers destroyed by severe earthquakes occurred in the last decades. The main reasons of the seismic vulnerability of these structures can be traced on their geometric and material features. In fact, the slenderness of the tower, i.e. the predominance of one dimension over the other two, is one of the main characteristics that determines the overall response [10, 11, 12]. Moreover, the constituent material, namely masonry, has an heterogeneous nature: several studies underlined that the proprieties of mortar and stone aggregates [13, 14, 15, 16], as well as variations in the quality of the construction work [17, 18], are important aspects affecting the seismic behavior. Other features, able to ensure a satisfactory global behavior, are the effectiveness of the connections among the external walls of the tower [19, 20] and between the vertical and horizontal structures [21, 22], as well as the presence of suitable elements such as ties, or buttresses [23] that counteract horizontal thrusts.

In this framework, the study of unreinforced masonry towers appears to be fundamental. Nowadays, a wide literature is available dealing with the analysis of these type of structures [24, 25, 26, 27]. The international debate on Cultural Heritage preservation pointed out the importance of performing effective and extensive experimental campaigns to assess the seismic vulnerability of masonry slender structures, such as towers [28, 29, 30, 31, 32, 33]. Several in-situ techniques exist and have been applied to historical buildings. Among others, it is worth mentioning non-destructive testing (NDT) methods, using for example georadar [29] or thermographic analysis [33] to assess damage, or slightly destructive methodologies, such as flat-jack tests, for the measurement of in-situ compressive stresses [32, 34]. However, as the realization of experiments is often a costly activity, during the last decades an increasing attention has been paid on the development of numerical tools and analytical models. The choice of the most appropriate approach depends on the desired level of accuracy and simplicity [35]. The most widely used numerical approach is the Finite Element Method (FEM). It shows different levels of complexity, concerning the geometrical discretization of the domain, ranging from 1D [36, 37] to 3D models [38], rather than plates and shells approaches [39]. FEM allows to perform different typologies of analysis, either static [40] or dynamic [41], and provides the adoption of a variety of constitutive equations describing the material behavior, i.e. no tension [37] or elasto-plastic [42] approaches, or models with damage [43]. Although FEM has been widely used for regular masonry structures, it appears to be limited in simulating irregular

*Corresponding author.
Email address: g-cusatis@northwestern.edu (Gianluca Cusatis)

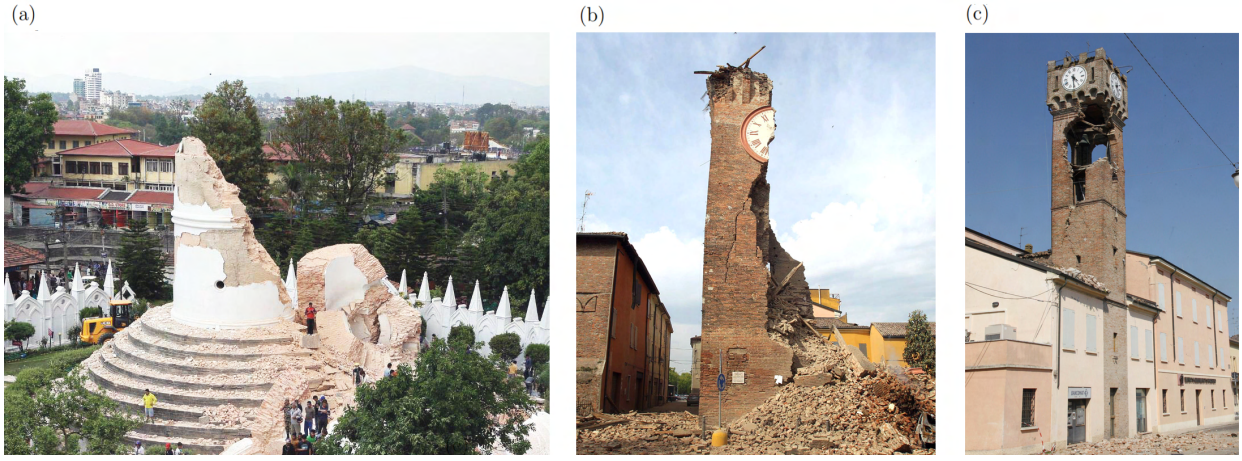

Figure 1: (a) Bhimsen Tower in Nepal, UNESCO patrimony; (b) Clock Tower in Finale Emilia, Emilia Romagna, Italy; (c) Tower in Novi, Modena, Italy.

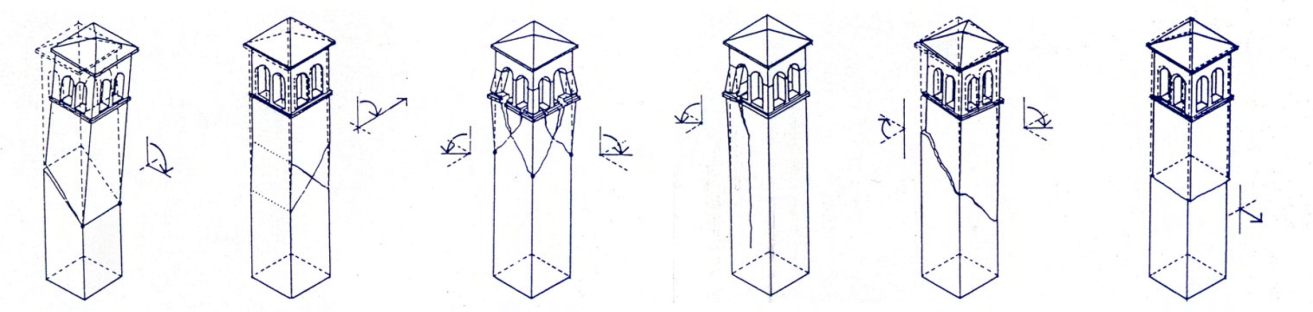

Figure 2: Recurrent fracturing patterns observed after seismic events in unreinforced masonry towers [1].

masonries. In fact, because of the heterogeneous nature of the material and the necessity of capturing complex crack distributions and fracture mechanisms, the use of a dedicate modeling tool is necessary.

For the assessment of seismic vulnerability, the Italian construction code [44] prescribes to perform analysis of local and global collapse mechanisms. The identification of the collapse mechanisms is not a trivial task and it requires a preliminary thorough study of the unreinforced masonry structure. The knowledge of the construction can be achieved through the performance of a complete survey that allows (i) the individuation of the different historical phases affecting the building modifications over the course of the years, and (ii) the full characterization of the structure both in terms of geometry and material [45]. With this perspective, it is possible to apply the procedure described by Giuffré in 1993 [46], who illustrated a methodology for the assessment of the vulnerability of unreinforced masonry structures. According to this work, the collapse mechanisms of the structure are identified a priori, by considering the involved portions of the building as a number of rigid blocks connected by unilateral hinges or sliding joints, in order to obtain a kinematic chain. Each rigid macro-

elements are assumed to have unlimited compressive strength and their reciprocal interfaces to be characterized by the absence of tensile strength. Thus, for each rigid block, the linear and non linear kinematic analyses should be applied and, therefore the mechanism most likely to occur of all the possible local mechanisms could be identified. Particularly, Fig. 2 shows that the aforementioned procedure is suitable to be applied to slender structures, such as masonry towers [47, 1, 48].

Although successful to some extent, this methodology shows three main limitations: (i) the choice of the collapse mechanisms is discretionary and affected by a certain level of uncertainty, (ii) both linear and non-linear kinematic analyses have to be applied to each rigid block, thus making this procedure tedious to be performed, (iii) the identification of simplified typology of collapse mechanism is inaccurate for complex geometries. In order to overcome these drawbacks, it is necessary to directly simulate the fracturing behavior of masonry towers. To this aim, several numerical methods can be used, as they capture the mechanical behavior of quasi-brittle materials with different degrees of complexity [49, 50]. The so-called Lattice Discrete Particle Model (LDPM) is here adopted to model the masonry fracturing behavior at the meso-scale. LDPM uniquely individuates the localization of crack pattern that triggers the collapse mechanism. In this way, the pre-definition of multiple collapse mechanisms can be avoided and the kinematic analysis can be directly applied to the individuated fractured structural configuration. Moreover, as the discrete model captures the entire damage evolution phenomena, starting from cracks localization, propagation up to the overall collapse, LDPM can be used as an alternative to the kinematic analysis [51]. In this study, the LDPM is used complementary with the kinematic analysis to describe the fracturing behavior of the Medici tower subjected to seismic excitation. The main characteristics of the fracture, occurred during the 2009 L'Aquila earthquake, is identified from the numerical results and, successively, the individuated cracked configuration is used to perform the linear kinematic analysis. Finally, a comparison between the kinematic analysis and the lattice discrete modeling is carried on, pointing out advantages and drawbacks of the proposed integrated approach.

2. Historical evolution of the Medici Tower

The Medici tower is located in Santo Stefano di Sessanio (L'Aquila, Italy), a urban aggregate belonging to the medieval period. The tower is believed to be one of the most representative architecture of the central Italy, because of its spectacular location in the landscape, on top of a hill, and within the core of the medieval town, as shown in Fig. 3a. Nowadays, the tower is the result of several modifications occurred along the centuries. It is fundamental observing that the knowledge of the historical phases affecting the building transformations is a fundamental prerequisite for any restoration intervention, including the choice of the most appropriate modeling strategy (see Section 4.2). Originally, during the 12th century, the cylindrical masonry tower was built without crowning on top. The hollow cylindri-

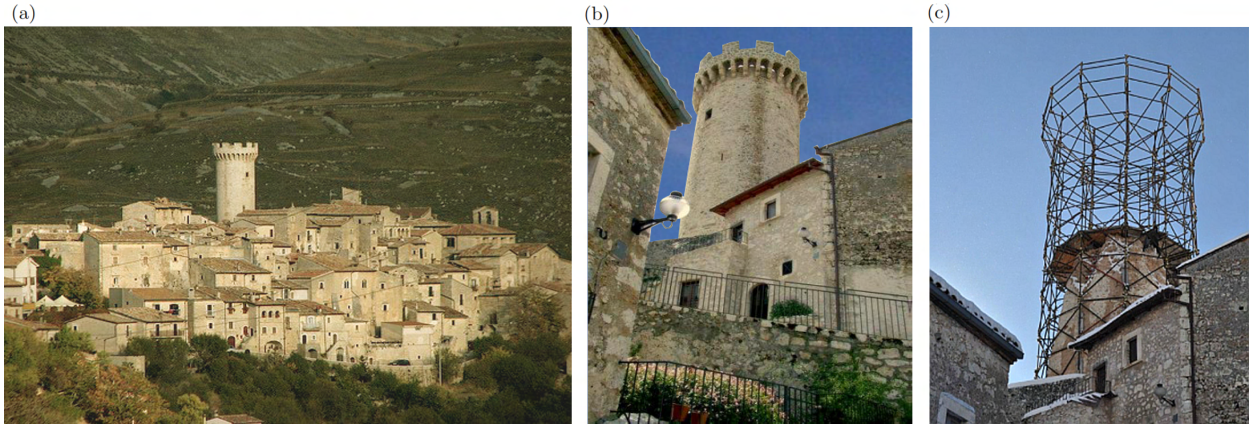

Figure 3: (a) Location of the Medici tower in the landscape and within the core of Santo Stefano di Sessanio; (b) architectonic configuration of the tower before the 2009 L'Aquila earthquake; (c) reproduction of the tower original profile through scaffolding and other prevention measures placed after the collapse in 2009.

cal cross section has an internal diameter of 3.86 m and a thickness of 1.50 m. In addition to the tower entrance, two small windows can be found along the body of the tower: one is located at a height of about 3.80 m from the bottom of the tower and the other consists of a narrow window placed near the top edge of the cylinder. During the period of the Angioins' domination, a crenellated masonry parapet was added to the upper portion of the tower, as shown in Fig. 3a and Fig. 3b. The battlement is characterized by 10 merlons and 30 machicolations and its function was to serve as real defence presidium for the village. In this way, the total height of the tower reached about 20 m. During the Second World War, the tower function changed, as it was used as antiaircraft station and, for this scope, a concrete slab was built on top of the tower. To exit the tower and access the crenellated parapet, a small window was opened in this floor. In April 2009, the tower did not resist the strong L'Aquila earthquake and collapsed almost completely. At present, just a stump of the bottom part of the original body remains, characterized by a variable height along its perimeter. The stump presents its shortest side in correspondence of the bottom window, at about 3.80 m height, and the tallest side in correspondence of the top window, at about 13 m height. After the 2009 L'Aquila earthquake, shoring, scaffolding and other prevention measures were placed around the ruins of the tower in order to prevent the falling of additional masonry pieces and to reproduce the original profile of the tower, as shown in Fig. 3c. For a more detailed description of the Medici tower, the reader is referred to Gregori and coworkers [52].

3. Main features of the April 2009 seismic event

On Monday, April the 6th, 2009, at 03:32:39 a.m. local time a devastating earthquake struck L'Aquila city and surrounding villages in the Abruzzo region of central Italy. The magnitude of the event was estimated to be M_L 5.8 (Richter magnitude scale), and M_W 6.2 (moment magnitude scale), according to the Italian National

Station [Id]	Record [Id]	Latitude [°]	Longitude [°]	Altitude [m]	Soil [-]	Epic. dist. [km]	PGA_{EW} [g]	PGA_{NS} [g]	PGA_Z [g]
AQG	FA030	42.37	13.34	721	B	4.3	0.42	0.43	0.22
AQV	GX066	42.38	13.34	692	C	4.8	0.67	0.56	0.51
AQK	AM043	42.34	13.40	726	B	5.6	0.34	0.34	0.35
AQA	CU104	42.38	13.34	693	C	5.8	0.39	0.45	0.38

Table 1: Station of the Accelerometric National Network located in proximity of the epicenter

Institute of Geophysics and Volcanology (INGV) [53]. The main shock was followed by a long-lasting seismic sequence, including more than 30 aftershocks with magnitude $3.5 < M_L < 5.0$. The earthquake has been interpreted as the result of a normal fault movement on a NW-SE oriented structure, about 15 km long, which is part of the 800 km long segmented normal fault system running all along the Apennines mountain chain [54, 55, 56]. Specifically, the entire area affected by the seismic activity covers an ellipse-shaped region parallel to the Apennines mountain belt, with principal axes of about 15 km long and secondary axes 2-5 km long. Several studies showed that the 2009 L'Aquila earthquake caused an up-dip slip movement with a rectangular rupture area of approximately 17x14 m^2, at a depth ranging between 11.8 km and 0.6 km. The rupture plane is characterized by a strike of 147°, a dip of 43° and a slip of 88° [57]. The main shaking was recorded by 55 stations of the National Accelerometric Network, fourteen being in the Abruzzo region. The nearest stations are AQG, AQV, AQK and AQA, located at 4.3 km, 4.8 km, 5.6 km and 5.8 km from the epicenter, respectively, on B- or C-type of soil (for the classification of soil types the reader is referred to [58]). Tab. 3 reports the values of the Peak Ground Acceleration (PGA) for the two horizontal and orthogonal directions (PGA_{EW} and PGA_{NS}) and for the vertical direction (PGA_Z).

4. Numerical analysis

The mechanical behavior of the Medici tower subjected to the 2009 L'Aquila earthquake is numerically analysed in this section. For this purpose, the Lattice Discrete Particle Model (LDPM) is here adopted.

4.1. The Lattice Discrete Particle Model

At first, the LDPM has been proposed by Cusatis and coworkers to simulate the behavior of concrete at a meso-scale level. This peculiarity has been achieved by modeling the interaction between coarse aggregate pieces [59, 60]. Afterwards, LDPM has been successfully adopted to capture the behavior of several quasi-brittle materials [61, 62, 63, 64, 65], and to simulate complex multi-physical phenomena such as aging, ASR [66, 67], and hygro-thermal-chemical processes [68, 69].

Particularly, LDPM allows the characterization of irregular masonry as two-phase material, i.e. stone-aggregate and mortar (Fig. 4a). The potential failure is assumed to occur at the aggregate-mortar interface or within the mortar layer [35], which is consistent with typical experimental observations on irregular masonry.

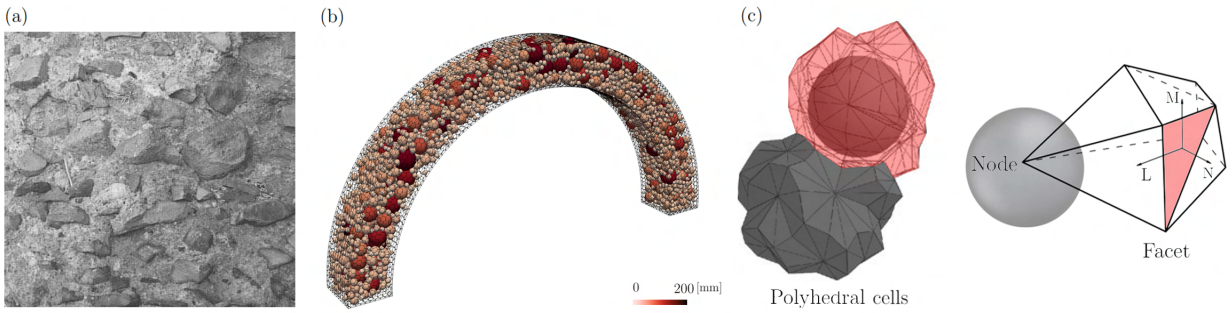

Figure 4: (a) Microstructure of irregular stone masonry; (b) aggregate distribution in a masonry arch; (c) two adjacent LDPM polyhedral cells enclosing the associated stone-aggregate pieces; tetrahedron portion associated with a stone-aggregate and a triangular LDPM facet.

The geometrical meso-structure of masonry is obtained through the following steps: (i) stone-aggregate pieces are assumed to be particles; they are randomly placed within the specimen volume through a trial and error procedure, from the largest to the smallest size. These particles or stones follow a particle size distribution function which is defined from a set of mix-design parameters: cement-mortar content c, water-to-mortar ratio w/c, maximum and minimum stone-aggregate size d_a and d_0, respectively, and Fuller coefficient n_f. Fig. 4b shows an example of particle placement inside the volume of a masonry semicircular arch; (ii) zero-radius particles are randomly placed on the external surface of the sample for the application of the boundary conditions; (iii) a Delaunay tetrahedralization procedure connects the centers of the spherical particles (or nodes), defining a lattice system; (iv) a three-dimensional domain tessellation is then performed, resulting in a system of polyhedral cells, each of which encloses a particle (Fig. 4c). The polyhedral cells form a network of triangular facets that are assumed to be the potential material failure location. The stones and the surrounding mortar are thus represented by irregular meso-cells that well idealize the real textures and shapes of typical masonry stones, and are intrinsically designed to produce a statistically isotropic masonry material often observed in real structures. Three sets of equations are written to complete the discrete model framework: definition of strains at each triangular facet, constitutive equations which relate facet strain vector with facet stress vector, and particle equilibrium equations. The constitutive equations describe a softening behavior for pure tension and shear-tension and a plastic hardening behavior for pure compression and shear-compression.

If $\mathbf{x}_i$ and $\mathbf{x}_j$ are the positions of nodes i and j, adjacent to the facet k, the facet strains are defined as:

$$\mathbf{e}_k = [e_N\, e_M\, e_L]^T = \left[\frac{\mathbf{n}_k^T[\![\mathbf{u}_k]\!]}{l}\ \frac{\mathbf{m}_k^T[\![\mathbf{u}_k]\!]}{l}\ \frac{\mathbf{l}_k^T[\![\mathbf{u}_k]\!]}{l}\right]^T \quad (1)$$

where e_N is the normal strain component, and e_M, e_L are the tangential strain components, $[\![\mathbf{u}_k]\!] = \mathbf{u}_j - \mathbf{u}_i$ is the displacement jump at the centroid of the facet k, $l = \|\mathbf{x}_j - \mathbf{x}_i\|_2$ is the distance between the two nodes, $\mathbf{n}_k = (\mathbf{x}_j - \mathbf{x}_i)/l$ and $\mathbf{m}_k$, $\mathbf{l}_k$ are two unit vectors mutually orthogonal in the facet plane projected orthogonally to the line connecting the adjacent nodes Fig. 1g. It was

demonstrated [70, 71, 72] that this definition of strains is completely consistent with classical strain definitions in continuum mechanics.

Similarly, one can define the traction vector as $\mathbf{t}_k = [t_N\ t_M\ t_L]^T$, where t_N is the normal component, t_M and t_L are the shear components. For the sake of readability, the subscript k that designates the facet is dropped in the following equations. In order to describe the behavior of the material, one needs to introduce the constitutive equations imposed at the centroid of each facet. The elastic behavior is defined through linear relations between the normal and shear stresses, and the corresponding strains as $t_N = E_N e_N$, $t_M = E_T e_M$ and $t_L = E_T e_L$, $E_N = E_0$ and $E_T = \alpha E_0$, $E_0 \approx E/(1-2\nu)$ and $\alpha \approx (1-4\nu)/(1+\nu)$ are the effective normal modulus and the shear-normal coupling parameter, respectively, and E is the macroscopic Young's modulus and ν is the macroscopic Poisson's ratio of the masonry.

In order to describe the inelastic behavior, one needs to distinguish three sets of mechanisms.

The first mechanism is the fracturing and cohesive behavior under tension and tension/shear occurring for $e_N > 0$. One can define the effective strain as $e = (e_N^2 + \alpha(e_M^2 + e_L^2))^{\frac{1}{2}}$, and the effective stress as $t = (t_N^2 + (t_M^2 + t_L^2)/\alpha)^{\frac{1}{2}}$ and write the relationship between stresses and strains through damage-type constitutive equations as $t_N = te_N/e$, $t_M = \alpha te_M/e$ and $t_L = \alpha te_L/e$ [73, 74].

The effective stress t is defined incrementally as $\dot{t} = E_N\dot{e}$ and its magnitude is limited by a strain-dependent boundary $0 \leqslant t \leqslant \sigma_{bt}(e,\omega)$ in which $\sigma_{bt}(e,\omega) = \sigma_0(\omega)\exp[-H_0(\omega)\langle e_{\max} - e_0(\omega)\rangle/\sigma_0(\omega)]$, $\langle x\rangle = \max(x,0)$, ω is a variable defining the degree of interaction between shear and normal loading defined as $\tan(\omega) = (e_N)/(\sqrt{\alpha}e_T) = (t_N\sqrt{\alpha})/(t_T)$; e_T is the total shear strain defined as $e_T = (e_M^2 + e_L^2)^{\frac{1}{2}}$, and t_T is the total shear stress defined as $t_T = (t_M^2 + t_L^2)^{\frac{1}{2}}$.

The maximum effective strain is time dependent and is defined as $e_{\max}(\tau) = (e_{N,\max}^2(\tau) + \alpha e_{T,\max}^2(\tau))^{\frac{1}{2}}$, where $e_{N,\max}(\tau) = \max_{\tau'<\tau}[e_N(\tau')]$ and $e_{T,\max}(\tau) = \max_{\tau'<\tau}[e_T(\tau')]$. The strength limit of the effective stress that defines the transition between pure tension and pure shear is

$$\sigma_0(\omega) = \sigma_t \frac{-\sin(\omega) + \sqrt{\sin^2(\omega) + 4\alpha\cos^2(\omega)/r_{st}^2}}{2\alpha\cos^2(\omega)/r_{st}^2} \tag{2}$$

where $r_{st} = \sigma_s/\sigma_t$ is the shear to tensile strength ratio, σ_s is the shear strength and σ_t is the tensile strength. The post-peak softening modulus is controlled by the effective softening modulus $H_0(\omega) = H_s/\alpha + (H_t - H_s/\alpha)(2\omega/\pi)^{n_t}$, in which $H_t = 2E_0/(l_t/l - 1)$, $H_s = r_s E_0$ and n_t is the softening exponent; l_t is the tensile characteristic length defined as $l_t = 2E_0 G_t/\sigma_t^2$, G_t is the mesoscale fracture energy.

The second set of equations describes the mechanism behind pore collapse and material compaction $e_N < 0$ under high confining pressures. The strain-hardening behavior in compression is simulated with the following strain-dependent boundary $\dot{t}_N = E_N\dot{e}_N$ and $-\sigma_{bc}(e_D, e_V) \leqslant t_N \leqslant 0$, where $\sigma_{bc} = \sigma_{c0} + H_c(-e_V - e_{c0})$ if $-e_V \leqslant e_{c1}$, otherwise $\sigma_{bc} = \sigma_{c1}\exp[(-e_V - e_{c1})H_c/\sigma_{c1}]$ and $H_c = H_{c1} + (H_{c0} - H_{c1})/(1 + \kappa_{c2}(r_{DV} -$

$\kappa_{c1}))$, $\sigma_{c1} = \sigma_{c0} + H_c(e_{c1} - e_{c0})$, $e_{c1} = \kappa_{c0}e_{c0}$, $e_{c0} = \sigma_{c0}/E_0$, $e_V = (V - V_0)/V_0$ is the volumetric strain computed at the LDPM tetrahedral level, $e_D = e_N - e_V$, $r_{DV} = |e_D|/(e_{V0} - e_V)$, for $e_D \leqslant 0$ and $r_{DV} = |e_D|/(e_{V0})$, for $e_D > 0$, $e_{V0} = 0.1e_{c0}$, σ_{c0} is the meso-scale yielding compressive stress, H_{c0} is the initial hardening modulus, and κ_{c0}, κ_{c1}, κ_{c2} are parameters governing the triaxial behavior at very high confinement.

The third failure type considered in LDPM describes the frictional behavior. In the presence of compressive stresses, the shear strength increases due to frictional effects. The frictional behavior is computed using a nonlinear Mohr-Coulomb model in which the internal friction coefficient varies from an initial value μ_0 to zero with the following formulation:

$$\sigma_{bs}(t_N) = \sigma_s + \mu_0\sigma_{N0} - \mu_0\sigma_{N0}\exp(t_N/\sigma_{N0}) \quad (3)$$

where σ_s is the cohesion and σ_{N0} is the so-called transitional stress.

Finally, the governing equations are completed by writing the equilibrium equations of each LDPM cell:

$$\sum_{k\in\mathcal{F}_I} A_k\mathbf{t}_k + V_I\mathbf{b} = \mathbf{0}, \quad \sum_{k\in\mathcal{F}_I} A_k\mathbf{c}_k \times \mathbf{t}_k = \mathbf{0} \quad (4)$$

where $\mathcal{F}_I$ is the set containing all the facets of a generic polyhedral cell I, A_k is the area of the facet k, $\mathbf{c}_k$ is the vector representing the distance between the center of the facet k and the center of the cell, V_I is the cell volume and $\mathbf{b}$ is the external body force applied to the cell.

4.2. Modeling strategy

4.2.1. The meso-scale characterization

The geometrical characterization of the LDPM mesostructure was calibrated in [75]. More specifically, the stone-to-mortar ratio $a/c = 3.4$ corresponding to the ratio between the volume of stones and the volume of cement-mortar, and the water-to-mortar ratio $w/c = 0.5$ were assumed based on the actual masonry composition. The cement-mortar content parameter $c = 427.5$ kg/m^3 was calculated such that the total mass density ρ were equal to 1,800.0 kg/m^3 using the formula: $\rho = c\,(1+w/c+a/c)$. The stones were assumed to have characteristic size within the range $d_0 = 33$ mm and $d_a = 200$ mm in order to simulate the coarse gravel. The Fuller coefficient $n_f = 0.5$ was assumed as default parameter since no specific sieve curve was assumed for the preparation of the specimens in the experimental campaign. The model parameters are as follows: normal elastic modulus $E_0 = 1{,}200$ MPa, shear-normal coupling parameter $\alpha = 0.065$, tensile strength $\sigma_t = 0.3$ MPa, tensile fracture energy $G_t = 11$ N/m, shear-to-tensile strength ratio $\sigma_s/\sigma_t = 1.25$, softening exponent $n_t = 0.2$, yielding compressive stress $\sigma_{c0} = 125$ MPa, initial hardening modulus $H_{c0}/E_0 = 0.4$, final hardening modulus $H_{c1} = 1$, transitional strain ratio $k_{c0} = 1.75$, deviatoric strain threshold ratio $k_{c1} = 1$, deviatoric damage parameter $k_{c2} = 5$, initial friction coefficient $\mu_0 = 0.2$, asymptotic friction coefficient $\mu_\infty = 0$, transitional stress $\sigma_{N0} = 42$ MPa, densification ratio $E_d/E_0 = 1$ and $r_s = 0$.

In order to accurately simulate the seismic behav-

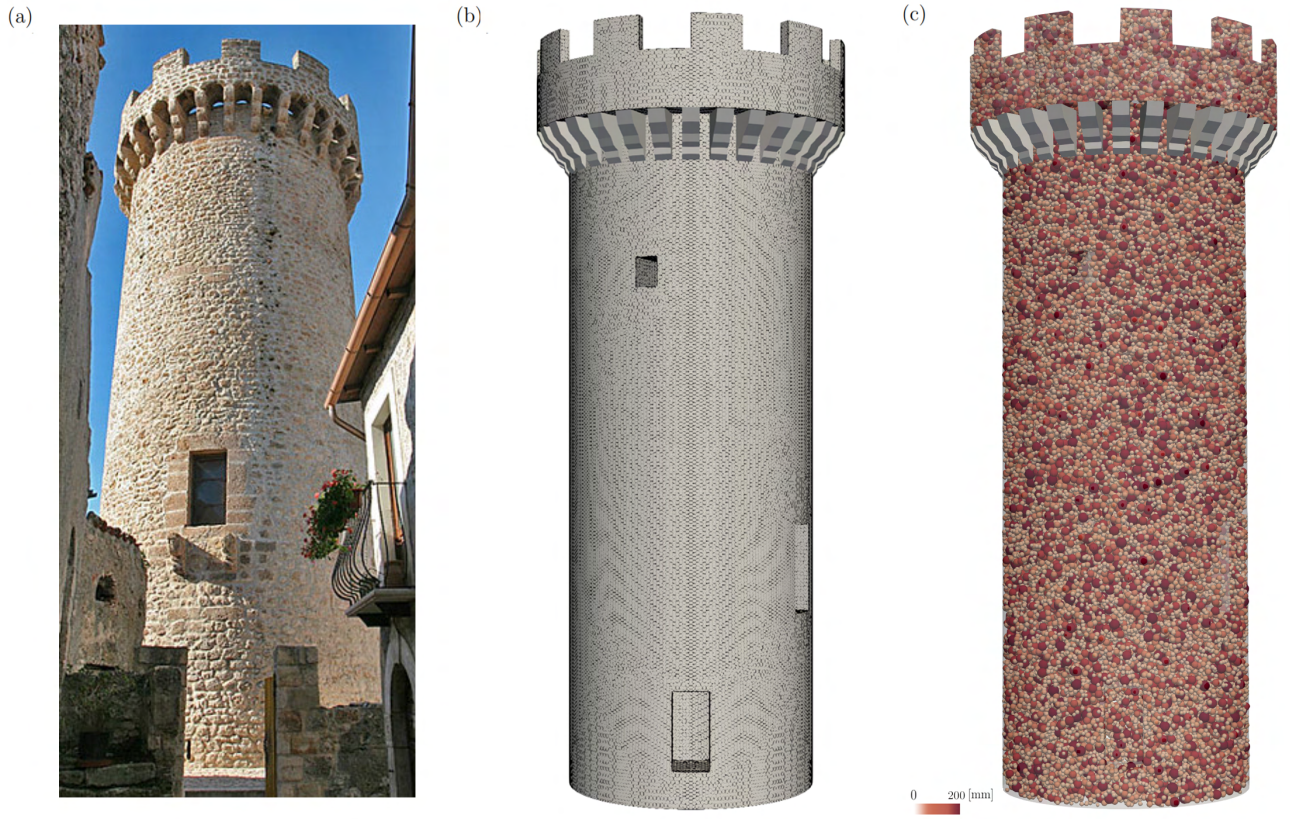

Figure 5: (a) Picture showing the Medici tower before the 2009 L'Aquila earthquake (USRC: Uff. Spec. Ric. Com. Cratere); LDPM mesh of the Medici tower showing: (b) the cell outline on the external cylindrical surface, (c) the distribution of spherical aggregates within the volume.

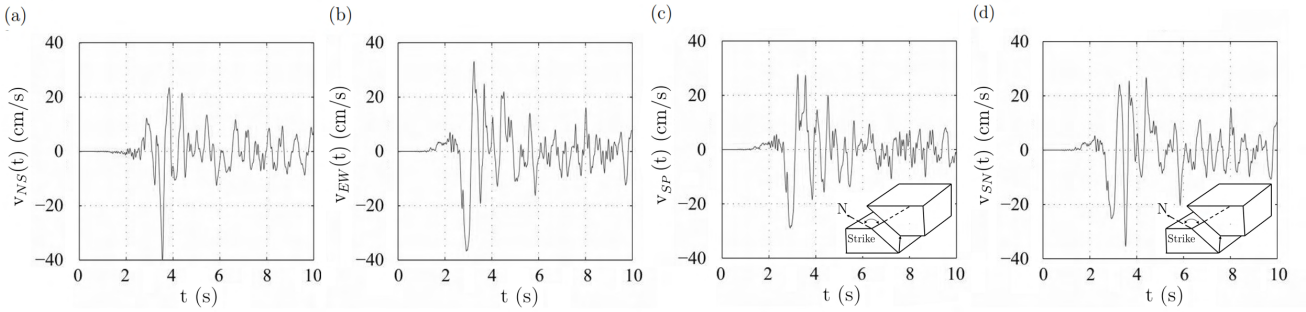

Figure 6: Histories of velocity along (a) the North-South direction, (b) the Est-West direction, (c) the parallel direction of the fault plane (Strike Parallel), (d) the normal direction of the fault plane (Strike Normal).

ior of the tower, the choice of the most suitable modeling strategy accounted for the several structural and functional modifications that affected the tower along the centuries. The sub-portions of the overall geometry are individuated to be representative of the real case of study (see Fig. 5a and Fig. 5b): the original hollow cylindrical body of the tower and the battlement composed by 10 merlons are modeled together using a single LDPM mesh (see Fig. 5b and Fig. 5c) in which the openings are included to reproduce the presence of the

windows. The 30 machicolations are conceived individually as elastic tetrahedral finite elements. The slab built on top of the tower is also modeled as a single elastic tetrahedron element. A penalty contact algorithm is used to connect the finite elements (namely the 30 machicolations and the top slab) to the main LDPM core (i.e. the body tower). The nodes belonging to the bottom surface of the tower are restrained by fixing all the rotations and the translations perpendicular to the direction of the seismic action. For all the simulations, three different LDPM meshes corresponding to three random stone distributions within the volume of the body tower are used. The presence of the self-weight is considered by preliminary applying the gravity loads.

4.2.2. Inputs for the seismic action

The load is imposed as a velocity in displacement control conditions and it is applied to a node list contained in a 500 mm height portion located at the bottom of the cylinder. For the benchmark case, the direction and the magnitude of the velocity are consistent with the ones of the 2009 L'Aquila earthquake and they are obtained following the procedure described in [76]. More specifically, the AQV accelerometric station, provides three histories of accelerations for the main shock of the L'Aquila seismic sequence, that are related to the North-South direction ($a_{NS}(t)$), the Est-West direction ($a_{EW}(t)$), and the vertical direction ($a_Z(t)$), respectively [77]. In general, knowing the evolution in time of the ground acceleration $a_i(t)$ for the generic direction i, it is possible to obtain the history of velocity related to the same direction $v_i(t)$ by integrating in time the history of acceleration: $v_i(t) = \int_{t_1}^{t_2} a_i(t)dt$. In this study, by neglecting the vertical component of the seismic action, and by considering a significant observation time of 10 seconds, one gets the histories of velocities in the North-South direction $v_{NS}(t)$ and in the Est-West direction $v_{EW}(t)$, as shown in Fig. 6a and Fig. 6b. Hence, the histories of velocities are projected along the parallel direction (Parallel Strike) and the orthogonal direction (Normal Strike) to the fault plane (see Fig. 6c and Fig. 6d). Finally, the magnitude of the velocity to be applied to the bottom of the cylinder has been set to 590 mm/s: its value is the summation between the two consecutive maximum Peaks Ground Velocities (PGV) taken in absolute value, i.e. 330 mm/s and 260 mm/s, as shown in Fig. 6d. Once the benchmark direction and magnitude of the velocity have been set to 147°of Strike (see Section 3) and 590 mm/s, other five cases are investigated, making varying either the magnitude or the direction of the velocity. Particularly, fixing the velocity direction to 147° with respect to the North-South axis, two magnitudes of velocity are considered, i.e. -330 mm/s and 260 mm/s, being the negative and positive maximum PGV, respectively. Moreover, fixing the velocity magnitude to 590 mm/s, three directions of velocity are considered, i.e. 15°, 45° and 90° with respect to the North-South axis, respectively.

4.3. Analysis of results and discussion

The results of the numerical simulations preformed on the benchmark case of Fig. 7a and Fig. 7b show that LDPM has the predictive capability of simulating the behavior of the tower under seismic excitation, show-

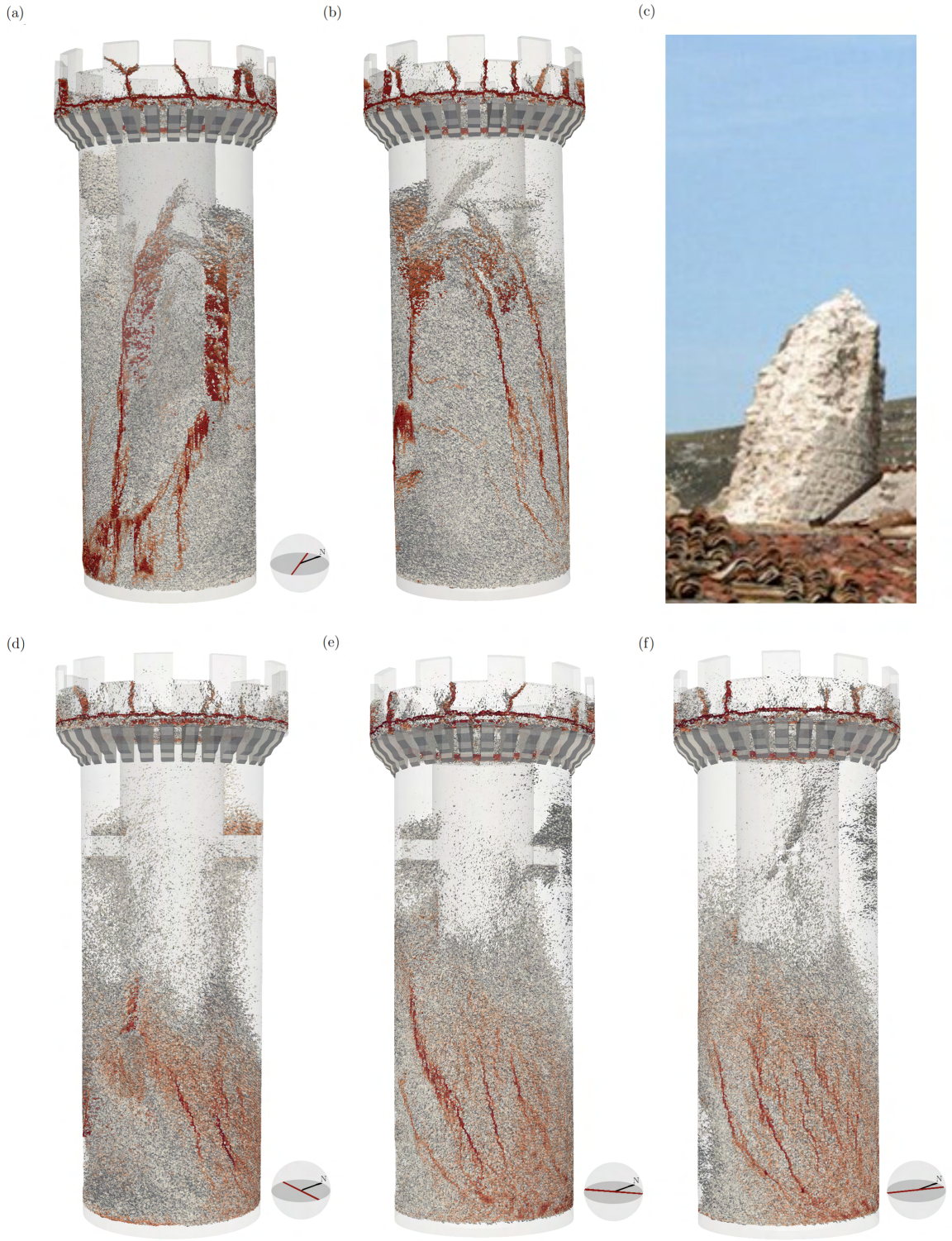

Figure 7: Cracked configuration in the Medici tower, perfectly simulating the failure occurred during the 2009 L'Aquila earthquake (a) in the South-Est facade; (b) in the North-West facade; (c) Tower stump after the 2009 L'Aquila earthquake; meso-scale crack openings assuming a direction of the seismic action rotated with respect to the North-South direction of: (d) 90°; (e) 45°; (f) 15°.

ing an excellent matching between the actual failure (in Fig. 7c) and the simulated ones (in Fig. 7a and Fig. 7b). In particular, the main contour of the mesoscale crack triggers from the bottom opening, and propagates diagonally reaching the top narrow window. This consideration suggests a correspondence between the type of failure and the presence of doors and windows, that interrupts the structural continuity of the masonry cylinder. For simple and compound geometries, Mercuri and coworkers [51] recently pointed out that the presence of openings greatly affects the seismic out-of-plane behavior of one- or two-story masonry walls, placed individually or collocated within the continuity of the facade. In that work, it has been demonstrated that the reductions of stiffness and bearing capacity are greater if the amount of opening within the wall increases. These observations appear to be realistic also for the description of the seismic behavior of complex geometries, as for the tower analyzed here. Thus, it is of primary relevance to account for the openings while considering the most suitable modeling strategy. It is also of paramount importance to observe diffused cracks at the top of the tower, with fractures extending all around the merlons of the battlement (see Fig. 7a and Fig. 7b). This phenomenon is probably caused by the motion of the rigid concrete slab built on top of the tower during the Second World War, when the tower was used as antiaircraft station. The slab, modeled using a single elastic finite element mesh, turned out to fall down almost untouched as consequence of the April 2009 earthquake. These results emphasize that the most appropriate modeling choices depend upon a deep knowledge of the building historical phases, achieved through profound cognitive investigations. In fact, ancient masonries are the results of several structural modifications along the centuries: the related functional changes affect the structural behavior and they have to be preliminary identified for the appropriate performance of numerical simulations.

Moreover, it worth mentioning that the simulated fracturing behavior of the tower mostly depends on the direction of the seismic action rather than the magnitude of the velocity, as shown in Fig. 7c, Fig. 7d and Fig. 7e. The fractured configurations related to the two cases with Strike fixed at 147° and PGV of 330 m/s and 260 m/s qualitatively coincide with the benchmark case (characterized by a PGV of 590 mm/s and shown in Fig. 7a and Fig. 7b) and, for the sake of brevity, they are not reported in this paper. On the other hand, Fig. 7 also reports the three different failure mechanisms of the tower, by setting the PGV to 590 mm/s and varying the direction of the seismic action. In particular, Fig. 7c, Fig. 7d and Fig. 7e show that the fractures become more diffused and almost vertical as the seismic direction rotates with respect to the North-South direction, of 90°, 45° and 15° respectively. The differences in the configuration of the fracturing patterns can be due to the variability in the relative position of the openings with respect to the direction of the seismic action. Overall, the LDPM shows a wide capability to capture the fracturing behavior up to the overall collapse of the structure for simple and complex geometries subjected to a variety of loading conditions.

5. The linear kinematic analysis

In this section, the linear kinematic analysis is applied to the structural configuration identified as benchmark case in Section 4.2 and Section 4.3, that reproduced the fracture pattern occurred during the 2009 L'Aquila earthquake. As already mentioned, the main contour is diagonal and it extends from the bottom opening to the top narrow window. For the kinematic analysis performed in this section, the crack is assumed to trigger from the bottom of the lower opening, at about 3.80 m from the ground, reaching the bottom of the top window, at about 13.00 m from the ground. According to [58], within the context of the linear kinematic analysis, the Life Safety Limit State (SLV) check for the generic mechanism is carried out by comparing the activating acceleration a_0^*, that represents the capacity of the structure, with the maximum expected spectral acceleration for the structure in ultimate conditions $a_{exp,SLV}$, that represents the demand:

$$a_0^* \geq a_{exp,SLV} \tag{5}$$

An alternative expression for the check of SLV Limit State consists in the following inequality, stating that the acceleration factor $f_{a,SLV}$ is greater than one:

$$f_{a,SLV} = \frac{a_0^*}{a_{exp,SLV}} \geq 1 \tag{6}$$

To evaluate the structural capacity, the activating acceleration a_0^* has to be computed. As a first step, the Virtual Work Theorem is applied by writing a work balance equation:

$$W_{E,S} + W_{E,G} = W_I \tag{7}$$

where $W_{E,S}$ is the external work done by seismic forces, $W_{E,G}$ is the external work done by gravity forces, and W_I is the work done by internal forces. In the case of rigid bodies, the internal work is set equal to zero, as no elastic/post-elastic deformation takes place. Developing the latter expression, the horizontal multiplier α_0 that activates the analyzed failure mode can be identified:

$$\alpha_0 \left(\sum_{i=1}^{n} m_{b,i}\delta_{x,i} + \sum_{i=n+1}^{n+m} m_{f,i}\delta_{x,i} \right) + g \sum_{i=1}^{n} m_{b,i}\delta_{y,i} = 0 \tag{8}$$

where n is the number of blocks of the kinematic chain, m is the number of internal floors, $m_{b,i}$ is the mass of the generic block, $m_{f,i}$ is the mass of the generic floor, $\delta_{x,i}$ is the virtual horizontal displacement of the point of application of the i-th seismic force and $\delta_{y,i}$ is the virtual vertical displacement of the i-th weight-force.

Finally, the activating acceleration a_0^* can be computed through the following equation:

$$a_0^* = \frac{\alpha_0 \sum_{i=1}^{n+m} m_i}{M^* F_C} = \frac{\alpha_0}{e^* F_C} \tag{9}$$

where m_i is the mass of the generic block or floor, F_C is the confidence factor accounting for the knowledge of the building, $e^* = M^* / \sum_{i=1}^{n} m_i$ is the participant mass ratio of the considered mechanism and M^* is the participant mass obtained as a function of the virtual displacements:

Table 2: Kinematic analytical parameters for the computation of the structural capacity.

Latitude [°]	Longitude [°]	α_0 [-]	e^* [-]	F_c [-]	a_0^* [m/s^2]
42.34	13.65	0.232	0.896	1.35	1.882

Table 3: Seismic parameters for the computation of the structural demand.

$a_{g,SLV}$ [g]	F_0 [-]	T_c^* [s]	T_1 [s]	S_S [-]	S_T [-]	S [-]	q [-]	$S_{e,SLV}(T_1)$ [g]	$a_{exp,SLV}$ [m/s^2]	$f_{a,SLV}$ [-]
0.256	2.365	0.344	0.404	1.16	1.40	1.62	1.75	4.07	2.33	0.809

$$M^* = \frac{\left(\sum_{i=1}^{n+m} m_i \delta_{x,i}\right)^2}{\sum_{i=1}^{n+m} m_i \delta_{x,i}^2} \tag{10}$$

Tab. 2 shows the values of the kinematic parameters adopted for the computation of the structural capacity.

Aiming to quantify the structural demand $a_{exp,SLV}$, the fundamental period of the structure T_1 is preliminary computed. With this purpose, several empirical formulas have been proposed trying to estimate the fundamental period of masonry towers as a function of their height H [58, 78, 79]. In particular, Ranieri and Fabbroncino [79] proposed a correlation between T_1 and H and compared the formula against a database of 30 Italian historical masonry towers, demonstrating that their expression provides the most accurate prediction for this specific structural typology. Hence, their formula will be adopted in this study:

$$T_1 = 0.013 H^{1.138} \tag{11}$$

If the activated portion lies directly on the foundation, $a_{exp,SLV}$ is evaluated as follows:

$$a_{exp,SLV} = \frac{a_{g,SLV} S}{q} \tag{12}$$

where $a_{g,SLV}$ is the reference PGA considered for a return period of 475 years, corresponding to the SLV Limit State, S is a correction factor accounting for the soil type and topography conditions, and q is the reduction factor that describes the ability of the system to dissipate energy in the non-elastic phase. The values of the aforementioned parameters are listed in Tab. 3 and they are computed according to [80, 58].

If the activated portion is located some distance above the foundation, an other expression has to be considered in addition to Eq. 12, accounting for the potential amplifications in acceleration due to the dynamic response of the structure. In this case, $a_{g,SLV}$ is the maximum of the two following expressions:

$$a_{exp,SLV} = \max \begin{cases} \frac{a_{g,SLV} S}{q} \\ \frac{S_{e,SLV}(T_1)\psi(z)\gamma}{q} \end{cases} \tag{13}$$

where $S_{e,SLV}(T_1)$ is the amplitude of the elastic spectrum corresponding to SLV Limit State, evaluated for the fundamental period of the structure T_1, $\psi(z) = z/H$ is the first vibration mode, approximated with a linear distribution along the height and normalized to one in correspondence of the building top, with z being the height of the kinematic hinge related to the considered

Figure 8: Geometrical configurations for linear kinematic analysis preformed assuming different diagonal fractures in function of the openings position y_W; the reader is referred to Tab. 4 for the detailed description of the cracked pattern.

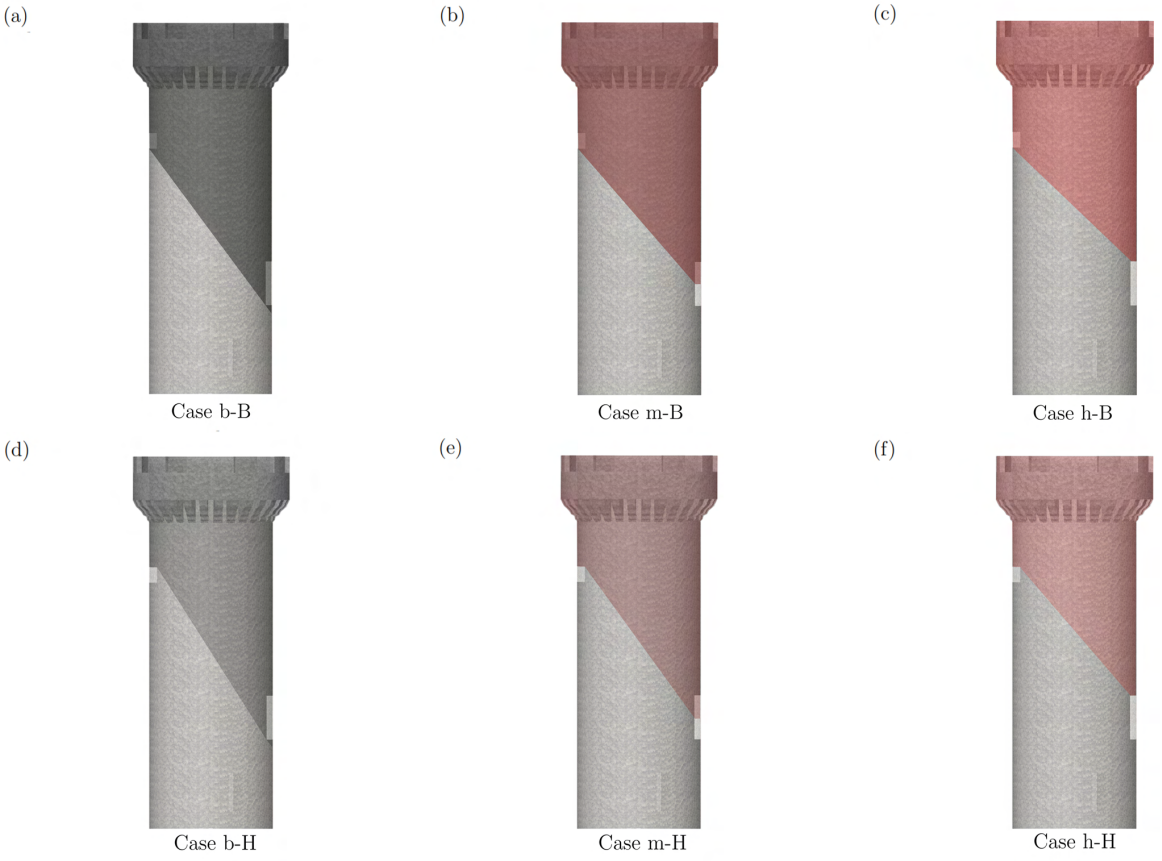

Case [Id]	Description fracture	y_{BW} [m]	y_{TW} [m]
b-B	from the bottom of the lower opening to the bottom of the higher window	3.80	13.00
m-B	from the middle of the lower opening to the bottom of the higher window	4.90	13.00
h-B	from the top of the lower opening to the bottom of the higher window	6.00	13.00
b-H	from the bottom of the lower opening to the top of the higher window	3.80	13.50
m-H	from the middle of the lower opening to the top of the higher window	4.90	13.50
h-H	from the top of the lower opening to the top of the higher window	6.00	13.50

Table 4: Geometrical parameters for the linear kinematic analysis.

mechanism with respect to the foundation and H the total height of the structure. In Eq. 13, the expression $\gamma = 3N/(2N + 1)$ represents the modal participation coefficient, where N is the number of the levels of the structure. It is worth noting that this simplified formula is applicable to structures that can be plausibly modeled with lumped masses located at the level of the floor connected by beam elements. Thus, the formula well approximates structural configurations whose floor masses are significantly greater than the masses of the vertical structures. For the Medici tower the vertical masonry structure is more massive than the floors

Table 5: Analytical parameters for the SLV limit state check.

Case [Id]	α_0 [-]	e^* [-]	F_c [-]	a_0^* [m/s^2]	$f_{a,SLV}$ [-]	SLV check
b-B	0.232	0.896	1.35	1.882	0.809	x
m-B	0.250	0.888	1.35	2.049	0.881	x
h-B	0.272	0.880	1.35	2.243	0.963	x
b-H	0.228	0.892	1.35	1.857	0.798	x
m-H	0.246	0.884	1.35	2.020	0.868	x
h-H	0.267	0.877	1.35	2.209	0.970	x

x = not satisfied

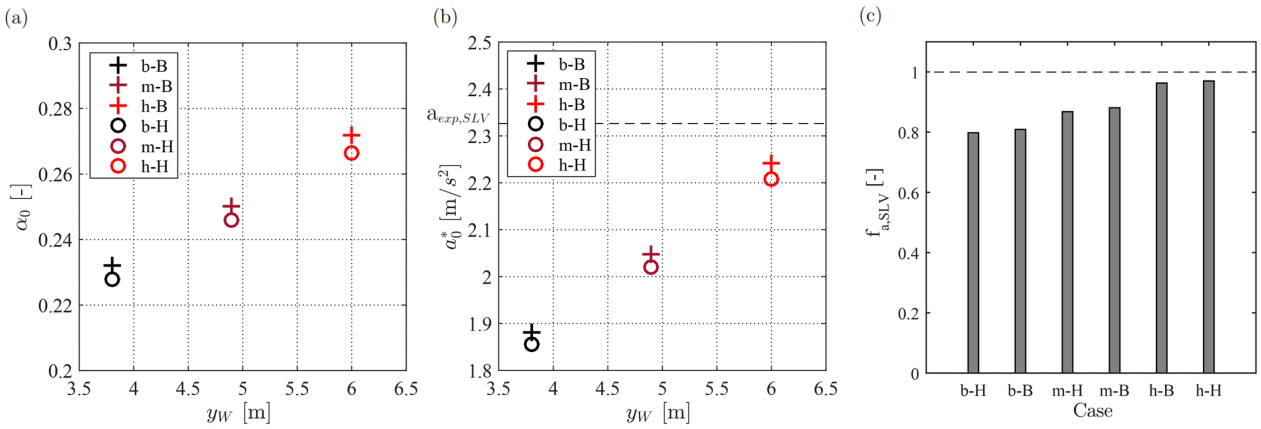

Figure 9: (a) Horizontal multiplier α_0 as a function of the openings position y_W; (b) activating acceleration a_0^* as a function of the openings position y_W.

and, therefore, a coefficient $N = 1$ is assumed. Thus, the modal participation coefficient turns out to be $\gamma = 1$, which means assuming that the first mode is the only one that significantly affects the acceleration $a_{exp,SLV}$. This assumption seems to be coherent with the simulated type of mechanism (shown in Fig. 7a and Fig. 7b) and the actual failure (see Fig. 7c). The values of the aforementioned parameters are listed in Tab. 3 and they are computed according to [80, 58]. Tab. 3 reports also the value of the acceleration factor ($f_{a,SLV}$=0.809) for the considered mechanism. Being $f_{a,SLV}$ less than 1, the SLV check is not verified and the collapse mechanism is activated.

6. Bridging LDPM with kinematic analysis

The results of the numerical simulations performed on the benchmark case of Fig. 7a and Fig. 7b showed that the main crack triggers from the bottom opening, and propagates diagonally reaching the top narrow window. Nevertheless, because of the heterogeneous nature of the masonry, the mutual position between the fracture contour and the openings is not clearly defined in the numerical results. On the other hand, the kinematic analysis performed in Sec. 5 assumed the diagonal crack to trigger from the bottom of the lower opening, at about 3.80 m from the ground, reaching the bottom of the top window, at about 13.00 m from the ground (Case b-B

in Fig. 8a). However, the randomness affecting the fracturing pattern should be considered while bridging the LDPM results with the kinematic analysis. With this aim, five additional cases (shown in Fig. 8 and Tab. 4) are analytically investigated by varying the reciprocal position between the diagonal fracture and the location of the openings. Fig. 8 illustrates the cracked configurations and Tab. 4 reports the geometrical parameters assumed for the linear kinematic analysis. The first set of three cases (cases b-B, m-B and h-B, corresponding to Fig. 8a, Fig. 8b and Fig. 8c, respectively) provides the diagonal crack to reach the bottom of the top window, at about 13.00 m from the ground, and to trigger from the bottom, the middle and the top of the lower opening, at 3.80 m, 4.90 m and 6.0 m from the ground, respectively. The second set of three cases (cases b-H, m-H and h-H, corresponding to Fig. 8d, Fig. 8e and Fig. 8f, respectively) assumes the diagonal crack to reach the top of the highest window, at about 13.50 m from the ground, and to trigger from the bottom, the middle and top of the lower opening, at 3.80 m, 4.90 m and 6.0 m from the ground, respectively.

The results of the kinematic analysis are reported in Tab. 5 and Fig. 9. For all the cases, the SLV check is not verified and the collapse mechanisms are activated. In fact, the activating acceleration a_0^* is always lower than the maximum expected spectral acceleration $a_{exp,SLV}$, as shown in Fig. 9b. Although the checks are not verified for all the cases, each one of them shows a different value of acceleration factor $f_{a,SLV}$, ranging from 0.798 to 0.970. In addition, a trend can be found: the acceleration factor $f_{a,SLV}$ increases as the position of the crack in the vicinity of the bottom opening is assumed to be located at the bottom, the middle, or at the top (see Fig. 9c). It is worth noting that the assumption made for the benchmark case, i.e. crack starting from the bottom of the bottom window to the bottom of the top window, is in favor of safety as the acceleration factor is one of the lowest among the six cases ($f_{a,SLV}$=0.809). The damage surveys following relevant seismic events brought to light recurring types of crack depending on the presence and the location of the openings within the masonry walls. For walls included within the continuity of the facade, one of the most recurrent observations of the damage consists in inclined cracks that propagate from the top of the bottom opening to the bottom of the top window and they are known in the field as the Saint Andrea Cross [81, 82]. For the tower analysed in this study, the results shown in Fig. 9c indicate that such an assumption does not lead to a calculation of the ultimate condition on the safest side. In fact, for the analyzed geometry (case Case h-B shown in Fig. 8c), the corresponding value of the acceleration factor is very close to the threshold value 1.0 ($f_{a,SLV}$=0.963), which questions the reliability of the SLV check.

The results demonstrate that the method proposed in this paper, i.e. identifying the main failure pattern from the lattice discrete modeling, and then performing and refining the simplified kinematic analysis, allows to obtain realistic ultimate conditions for a given geometry. However, in other situations, it appears difficult or impossible to proceed this way, as the damage cannot

be described by a single crack. For instance, Fig. 7c, Fig. 7d and Fig. 7e showed that the fracture becomes less localized and more distributed as the seismic direction changes. Similar conclusions have been reached in the work of Mercuri and coworkers [51]: in the most general case, it is necessary to analyze the fracturing and the collapse behavior of masonry structures with elaborate numerical models, such as LDPM, in addition to simplified kinematic analysis.

7. Summary and conclusions

Due to their slender geometry and the brittle heterogeneous nature of their constituent material, ancient masonry towers are highly vulnerable to seismic actions. The mechanical response, the induced damage, and the eventual collapse mechanism due to the action of the earthquake depend on the geometrical features and properties of masonry. In order to calculate the ultimate conditions of these towers, kinematic analyses are most often performed. Building codes usually require the identification of collapse mechanisms, which in turns require a preliminary thorough survey of the analyzed structure. In this study, a comprehensive numerical model, namely the Lattice Discrete Particle Model, is adopted to model the masonry fracturing behavior and predict the most likely to occur collapse mechanism. The information about crack distribution and location are then used to define the fractured structural configuration in the kinematic analysis. This paper incorporates this method to investigate the fracturing behavior of the Medici tower subjected to the seismic excitation due to the 2009 L'Aquila earthquake. Crack contours are simulated and six different failure locations are assumed for the kinematic analysis. The obtained results suggest the following conclusions:

- The failure of the Medici tower under seismic excitation is numerically well replicated by LDPM.
- The failure pattern greatly depend on the direction of the seismic action.
- The kinematic analysis performed with six different configurations underline the importance of identifying the correct collapse mechanism to obtain more reliable SLV checks.

The proposed method is successful in analyzing the ultimate condition of the Medici tower. It appears however that in other cases, for instance if different directions of the seismic action are assumed, the use of simplified kinematic analyses is only a crude approximation. In fact, these situations call for advanced numerical models capable of accurately capturing fracture propagation and crack distribution in order to assess the vulnerability of existing masonry structures.

References

[1] G. nazionale per la difesa dai terremoti, F. Doglioni, A. Moretti, V. Petrini, Le chiese e il terremoto: dalla vulnerabilità constatata nel terremoto del Friuli al miglioramento antisismico nel restauro, verso una politica di prevenzione, Lint, 1994.

[2] P. Mendes, M. Baptista, L. Agostinho, S. Lagomarsino, J. Costav, Structural and dynamic analysis of n. sra. do carmo church, lagos portugal, Proceedings EURODYN2005, Structural Dynamics (2005) 311–318.

[3] G. Osmancikli, Ş. Uçak, F. N. Turan, T. Türker, A. Bayraktar, Investigation of restoration effects on the dynamic characteristics of the hagia sophia bell-tower by ambient vibration test, Construction and Building Materials 29 (2012) 564–572.

[4] S. DelloRusso, G. Juneja, B. Gabby, D. Dusenberry, Monitoring and repair of the milwaukee city hall masonry tower, Journal of performance of constructed facilities 22 (4) (2008) 197–206.

[5] M. Pieraccini, D. Dei, M. Betti, G. Bartoli, G. Tucci, N. Guardini, Dynamic identification of historic masonry towers through an expeditious and no-contact approach: Application to the "torre del mangia" in siena (italy), Journal of Cultural Heritage 15 (3) (2014) 275–282.

[6] G. Bartoli, M. Betti, S. Giordano, In situ static and dynamic investigations on the "torre grossa" masonry tower, Engineering Structures 52 (2013) 718–733.

[7] G. Russo, O. Bergamo, L. Damiani, D. Lugato, Experimental analysis of the "saint andrea" masonry bell tower in venice. a new method for the determination of "tower global young's modulus e", Engineering structures 32 (2) (2010) 353–360.

[8] S. Lagomarsino, Damage assessment of churches after l'aquila earthquake (2009), Bulletin of Earthquake Engineering 10 (1) (2012) 73–92.

[9] M. Poiani, V. Gazzani, F. Clementi, G. Milani, M. Valente, S. Lenci, Iconic crumbling of the clock tower in amatrice after 2016 central italy seismic sequence: advanced numerical insight, Procedia Structural Integrity 11 (2018) 314–321.

[10] K. Lang, H. Bachmann, On the seismic vulnerability of existing unreinforced masonry buildings, Journal of Earthquake Engineering 7 (03) (2003) 407–426.

[11] P. Morandi, G. Magenes, Second order effects in out-of-plane strength of urm walls subjected to bending and compression, ROSE Report (2006).

[12] T. M. Ferreira, A. A. Costa, A. Costa, Analysis of the out-of-plane seismic behavior of unreinforced masonry: A literature review, International Journal of Architectural Heritage 9 (8) (2015) 949–972.

[13] S. Casolo, G. Uva, Nonlinear analysis of out-of-plane masonry façades: full dynamic versus pushover methods by rigid body and spring model, Earthquake Engineering & Structural Dynamics 42 (4) (2013) 499–521.

[14] G. D. Felice, R. Giannini, Out-of-plane seismic resistance of masonry walls, Journal of earthquake engineering 5 (02) (2001) 253–271.

[15] G. de Felice, Out-of-plane seismic capacity of masonry depending on wall section morphology, International Journal of Architectural Heritage 5 (4-5) (2011) 466–482.

[16] A. Giuffrè, A mechanical model for statics and dynamics of historical masonry buildings, in: Protection of the architectural heritage against earthquakes, Springer, 1996, pp. 71–152.

[17] P. B. Lourenço, J. G. Rots, Multisurface interface model for analysis of masonry structures, Journal of engineering mechanics 123 (7) (1997) 660–668.

[18] V. Giamundo, V. Sarhosis, G. Lignola, Y. Sheng, G. Manfredi, Evaluation of different computational modelling strategies for the analysis of low strength masonry structures, Engineering Structures 73 (2014) 160–169.

[19] A. A. Costa, A. Arêde, A. Costa, C. S. Oliveira, In situ cyclic tests on existing stone masonry walls and strengthening solutions, Earthquake Engineering & Structural Dynamics 40 (4) (2011) 449–471.

[20] A. A. Costa, A. Arêde, A. Costa, C. S. Oliveira, Out-of-plane behaviour of existing stone masonry buildings: experimental evaluation, Bulletin of Earthquake Engineering 10 (1) (2012) 93–111.

[21] D. D'Ayala, E. Speranza, Definition of collapse mechanisms and seismic vulnerability of historic masonry buildings, Earthquake Spectra 19 (3) (2003) 479–509.

[22] M. R. Valluzzi, On the vulnerability of historical masonry structures: analysis and mitigation, Materials and structures 40 (7) (2007) 723–743.

[23] E. Spacone, V. Sepe, E. Raka, Safety assessment of masonry building aggregates in poggio picenze, following the l'aquila 2009 earthquake, in: 15th world conference on earthquake engineering, Lisbon, 2012.

[24] S. Ivorra, F. J. Pallarés, Dynamic investigations on a masonry bell tower, Engineering structures 28 (5) (2006) 660–667.

[25] D. Abruzzese, L. Miccoli, J. Yuan, Mechanical behavior of leaning masonry huzhu pagoda, Journal of cultural heritage 10 (4)

(2009) 480–486.

[26] M. Valente, G. Milani, Seismic assessment of historical masonry towers by means of simplified approaches and standard fem, Construction and Building Materials 108 (2016) 74–104.

[27] V. Sarhosis, G. Milani, A. Formisano, F. Fabbrocino, Evaluation of different approaches for the estimation of the seismic vulnerability of masonry towers, Bulletin of Earthquake Engineering 16 (3) (2018) 1511–1545.

[28] I. Committee, et al., Recommendations for the analysis, conservation and structural restoration of architectural heritage, See www. icomos. org (2005).

[29] L. Binda, L. Zanzi, M. Lualdi, P. Condoleo, The use of georadar to assess damage to a masonry bell tower in cremona, italy, Ndt & e International 38 (3) (2005) 171–179.

[30] P. B. Lourenço, Assessment, diagnosis and strengthening of outeiro church, portugal, Construction and Building Materials 19 (8) (2005) 634–645.

[31] C. Modena, M. Valluzzi, R. T. Folli, L. Binda, Design choices and intervention techniques for repairing and strengthening of the monza cathedral bell-tower, Construction and Building Materials 16 (7) (2002) 385–395.

[32] A. Anzani, L. Binda, A. Carpinteri, S. Invernizzi, G. Lacidogna, A multilevel approach for the damage assessment of historic masonry towers, Journal of Cultural Heritage 11 (4) (2010) 459–470.

[33] A. Carpinteri, S. Invernizzi, G. Lacidogna, In situ damage assessment and nonlinear modelling of a historical masonry tower, Engineering Structures 27 (3) (2005) 387–395.

[34] A. Carpinteri, S. Invernizzi, G. Lacidogna, Historical brickmasonry subjected to double flat-jack test: Acoustic emissions and scale effects on cracking density, Construction and Building Materials 23 (8) (2009) 2813–2820.

[35] P. Lourenço, Computational strategy for masonry structures, Delft University of Technology and DIANA Research (1996).

[36] P. Riva, F. Perotti, E. Guidoboni, E. Boschi, Seismic analysis of the asinelli tower and earthquakes in bologna, Soil Dynamics and Earthquake Engineering 17 (7-8) (1998) 525–550.

[37] K. Bernardeschi, C. Padovani, G. Pasquinelli, Numerical modelling of the structural behaviour of buti's bell tower, Journal of Cultural Heritage 5 (4) (2004) 371–378.

[38] S. Casolo, A three-dimensional model for vulnerability analysis of slender medieval masonry towers, Journal of Earthquake Engineering 2 (04) (1998) 487–512.

[39] S. Casolo, G. Milani, G. Uva, C. Alessandri, Comparative seismic vulnerability analysis on ten masonry towers in the coastal po valley in italy, Engineering Structures 49 (2013) 465–490.

[40] M. Bocciarelli, G. Barbieri, A numerical procedure for the pushover analysis of masonry towers, Soil Dynamics and Earthquake Engineering 93 (2017) 162–171.

[41] A. M. Marra, L. Salvatori, P. Spinelli, G. Bartoli, Incremental dynamic and nonlinear static analyses for seismic assessment of medieval masonry towers, Journal of Performance of Constructed Facilities 31 (4) (2017) 04017032.

[42] G. Milani, S. Russo, M. Pizzolato, A. Tralli, Seismic behavior of the san pietro di coppito church bell tower in l'aquila, italy, The Open Civil Engineering Journal 6 (1) (2012).

[43] F. Peña, P. B. Lourenço, N. Mendes, D. V. Oliveira, Numerical models for the seismic assessment of an old masonry tower, Engineering Structures 32 (5) (2010) 1466–1478.

[44] Decreto del ministro delle infrastrutture 17 gennaio 2018. aggiornamento delle "norme tecniche per le costruzioni", Gazzetta Ufficiale della Repubblica Italiana.

[45] C. Brandi, Teoria del restauro, Ed. di storia e letteratura, 1963.

[46] A. Giuffrè, Sicurezza e conservazione dei centri storici, Il caso Ortigia (1993) 279.

[47] G. Bartoli, M. Betti, A. Vignoli, A numerical study on seismic risk assessment of historic masonry towers: a case study in san gimignano, Bulletin of Earthquake Engineering 14 (6) (2016) 1475–1518.

[48] V. Sepe, E. Speranza, A. Viskovic, A method for large-scale vulnerability assessment of historic towers, Structural Control and Health Monitoring: The Official Journal of the International Association for Structural Control and Monitoring and of the European Association for the Control of Structures 15 (3) (2008) 389–415.

[49] Z. P. Bazant, Fracture and size effect in concrete and other quasibrittle materials, Routledge, 2019.

[50] G. Cusatis, L. Cedolin, Two-scale study of concrete fracturing

behavior, Engineering Fracture Mechanics 74 (1-2) (2007) 3–17.

[51] M. Mercuri, M. Pathirage, A. Gregori, G. Cusatis, Computational modeling of the out-of-plane behavior of unreinforced irregular masonry, Engineering Structures 223 (2020) 111181.

[52] A. Gregori, H. Salem, T. Harak, K. Fassieh, A. Khalil, Collapse analysis of santo stefano tower using applied element method, in: Proceedings of 16th world conference on earthquake engineering, 16WCEE, 2017.

[53] I. N. di Geofisica e Vulcanologia, The l'aquila seismic sequence, april 2009, http://www.ingv.it.

[54] G. Ameri, P. Augliera, D. Bindi, E. D'Alema, C. Ladina, S. Lovati, L. Luzi, S. Marzorati, M. Massa, F. Pacor, et al., Strong-motion parameters of the mw= 6.3 abruzzo (central italy) earthquake (2009).

[55] E. Chioccarelli, F. De Luca, I. Iervolino, Preliminary study of l'aquila earthquake ground motion records v5. 20, ReLuis Report, http://www. reluis. it (2009).

[56] L. Decanini, L. Liberatore, F. Mollaioli, G. Monti, O. Al Shawa, Studio preliminare della domanda sismica elastica ed anelastica in termini di energia, spostamento e forze (rel. 1.0), Web report available at http://www. reluis. it (2009).

[57] E. Chioccarelli, I. Iervolino, Direttività e azione sismica: discussione per l'evento de l'aquila, Convegno Anidis (2009).

[58] I. Code-NTC18, Norme tecniche per le costruzioni in zone sismiche, Ministerial Decree DM (2018).

[59] G. Cusatis, D. Pelessone, A. Mencarelli, Lattice discrete particle model (ldpm) for failure behavior of concrete. i: Theory, Cement and Concrete Composites 33 (9) (2011) 881–890.

[60] G. Cusatis, A. Mencarelli, D. Pelessone, J. Baylot, Lattice discrete particle model (ldpm) for failure behavior of concrete. ii: Calibration and validation, Cement and Concrete composites 33 (9) (2011) 891–905.

[61] W. Li, R. Rezakhani, C. Jin, X. Zhou, G. Cusatis, A multiscale framework for the simulation of the anisotropic mechanical behavior of shale, International Journal for Numerical and Analytical Methods in Geomechanics 41 (14) (2017) 1494–1522.

[62] R. Rezakhani, X. Zhou, G. Cusatis, Adaptive multiscale homogenization of the lattice discrete particle model for the analysis of damage and fracture in concrete, International Journal of Solids and Structures 125 (2017) 50–67.

[63] C. Ceccato, M. Salviato, C. Pellegrino, G. Cusatis, Simulation of concrete failure and fiber reinforced polymer fracture in confined columns with different cross sectional shape, International Journal of Solids and Structures 108 (2017) 216–229.

[64] E. A. Schauffert, G. Cusatis, Lattice discrete particle model for fiber-reinforced concrete. i: Theory, Journal of Engineering Mechanics 138 (7) (2011) 826–833.

[65] J. Smith, G. Cusatis, D. Pelessone, E. Landis, J. O'Daniel, J. Baylot, Discrete modeling of ultra-high-performance concrete with application to projectile penetration, International Journal of Impact Engineering 65 (2014) 13–32.

[66] M. Alnaggar, G. Cusatis, G. Di Luzio, Lattice discrete particle modeling (ldpm) of alkali silica reaction (asr) deterioration of concrete structures, Cement and Concrete Composites 41 (2013) 45–59.

[67] M. Pathirage, F. Bousikhane, M. D'Ambrosia, M. Alnaggar, G. Cusatis, Effect of alkali silica reaction on the mechanical properties of aging mortar bars: Experiments and numerical modeling, International Journal of Damage Mechanics 28 (2) (2019) 291–322.

[68] G. Di Luzio, G. Cusatis, Hygro-thermo-chemical modeling of high performance concrete. i: Theory, Cement and Concrete composites 31 (5) (2009) 301–308.

[69] M. Pathirage, D. Bentz, G. Di Luzio, E. Masoero, G. Cusatis, The onix model: a parameter-free multiscale framework for the prediction of self-desiccation in concrete, Cement and Concrete Composites 103 (2019) 36–48.

[70] G. Cusatis, E. Schauffert, Discontinuous cell method (dcm) for cohesive fracture propagation, in: Proceedings of the 7th international conference on fracture mechanics of concrete and concrete structures (FraMCos 7), Vol. 845, 2010, pp. 23–28.

[71] R. Rezakhani, G. Cusatis, Generalized mathematical homogenization of the lattice discrete particle model, in: 8th International Conference on Fracture Mechanics of Concrete and Concrete Structures, FraMCoS 2013, 2013, pp. 261–271.

[72] G. Cusatis, X. Zhou, High-order microplane theory for quasi-brittle materials with multiple characteristic lengths, Journal of

Engineering Mechanics 140 (7) (2013) 04014046.

[73] G. Cusatis, Z. P. Bažant, L. Cedolin, Confinement-shear lattice model for concrete damage in tension and compression: I. theory, Journal of Engineering Mechanics 129 (12) (2003) 1439–1448.

[74] G. Cusatis, Z. P. Bažant, L. Cedolin, Confinement-shear lattice model for concrete damage in tension and compression: Ii. computation and validation, Journal of Engineering Mechanics 129 (12) (2003) 1449–1458. doi:10.1061/(ASCE)0733-9399(2003)129:12(1449).

[75] M. Angiolilli, A. Gregori, M. Pathirage, G. Cusatis, Fiber reinforced cementitious matrix (frcm) for strengthening historical stone masonry structures: Experiments and computations, Engineering Structures 224 (2020) 111102.

[76] L. Decanini, L. Liberatore, F. Mollaioli, G. Monti, O. Al Shawa, Terremoto aquilano del 6 aprile 2009 studio preliminare della domanda sismica elastica ed anelastica in termini di energia, spostamenti e forze (rel. 1.0) (2009).

[77] L. Decanini, L. Liberatore, F. Mollaioli, Damage potential of the 2009 l'aquila, italy, earthquake, Journal of Earthquake and Tsunami 6 (03) (2012) 1250032.

[78] M. per i Beni, et al., Linee guida per la valutazione e riduzione del rischio del patrimonio culturale: Allineamento alle nuove Norme tecniche per le costruzioni, Gangemi Editore spa, 2011.

[79] C. Rainieri, G. Fabbrocino, Il periodo elastico delle torri in muratura: correlazioni empiriche per la previsione, in: XIV Congresso Nazionale L'Ingegneria Sismica in Italia, Bari, 2011, pp. 18–22.

[80] C. Applicativa delle NTC18, Circolare del ministero delle infrastrutture e dei trasporti 21 gennaio 2019, n7 recante istruzioni per l'applicazione delle nuove norme tecniche per le costruzioni di cui al decreto ministeriale 20 febbraio 2018, Suppl ord (2019).

[81] G. Magenes, A. Penna, I. E. Senaldi, M. Rota, A. Galasco, Shaking table test of a strengthened full-scale stone masonry building with flexible diaphragms, International Journal of Architectural Heritage 8 (3) (2014) 349–375.

[82] G. Magenes, A. Penna, A. Galasco, A full-scale shaking table test on a two-storey stone masonry building, in: 14th European Conference on Earthquake Engineering, 2010.